Diagnosing ozone-NO$_x$-VOC sensitivity and revealing causes of ozone increases in China based on 2013-2021 satellite retrievals

Jie Ren[1], Fangfang Guo[1], and Shaodong Xie[1]

[1]State Key Joint Laboratory of Environmental Simulation and Pollution Control, College of Environmental Sciences and Engineering, Peking University, Beijing, 100871, China

Correspondence to: Shaodong Xie (sdxie@pku.edu.cn)

Abstract. Particulate matter (PM$_{2.5}$) concentrations in China have decreased significantly in recent years, but surface ozone (O$_3$) concentrations showed upward trends at more than 71% of air quality monitoring stations from 2015 to 2021. To reveal the causes of O$_3$ increases, O$_3$ production sensitivity is accurately diagnosed by deriving regional threshold values of satellite tropospheric formaldehyde-to-NO$_2$ ratio (HCHO/NO$_2$), and O$_3$ responses to precursors changes are evaluated by tracking volatile organic compounds (VOCs) and NO$_x$ with satellite HCHO and NO$_2$. Results showed that the HCHO/NO$_2$ ranges of transition from VOC-limited to NO$_x$-limited regimes vary apparently among Chinese regions. VOC-limited regimes are widespread found over megacity clusters (North China Plain, Yangtze River Delta, and Pearl River Delta) and concentrated in developed cities (such as Chengdu, Chongqing, Xi'an, and Wuhan). NO$_x$-limited regimes dominate most of the remaining areas. From 2013 to 2021, satellite NO$_2$ and HCHO columns showed an annual decrease of 3.7% and an increase of 0.1%, respectively, indicating an effective reduction in NO$_x$ emissions but a failure reduction of VOC emissions. This finding further shows that O$_3$ increases in major cities occur because the Clean Air Action Plan only reduces NO$_x$ emissions without effective VOC control. Two cases in Beijing and Chengdu also verified that NO$_x$ reduction alone or VOC increase leads to O$_3$ increases. Based on the O$_3$–NO$_x$–VOC relationship by satellite NO$_2$ and HCHO in Beijing, Chengdu, and Guangzhou, the ozone concentration can be substantially reduced if the reduction ratio of VOCs/NO$_x$ is between 2:1 and 4:1.

1 Introduction

China has been dedicating to fighting against air pollution in the past years. Since the Chinese government implemented the Air Pollution Prevention and Control Action Plan in 2013, the ambient concentration of particulate matter with aerodynamic diameter of <2.5 μm ($PM_{2.5}$) has decreased significantly (Jiang et al., 2020; Xiao et al., 2021); however, ozone (O_3) pollution remains severe or even continues to worsen at least until 2019 (Lu et al., 2020; Zhao et al., 2020). Ozone pollution has restricted the continuous improvement of China's air quality. Thus, it has attracted widespread attention from the government, scientists, and the public.

Tropospheric ozone is produced by photochemical oxidation of volatile organic compounds (VOCs) in the presence of nitrogen oxides (NO_x: $NO + NO_2$) (Atkinson, 2000). However, the O_3 responses to NO_x and VOC reduction are not linear. The O_3 formation throughout much of the troposphere is largely controlled by the availability of NO_x (NO_x-limited), but in regions with high NO_x emissions, such as metropolitan areas, O_3 formation can be VOC-limited or transform between regimes (Sillman and He, 2002; KLEINMAN, 1994). A VOC-limited regime means that reducing VOC emissions can result in low O_3 production; in the presence of high NO_x, reduction of NO_x emissions alleviates ozone titration and even leads to ozone increases (Sillman, 1999). Local O_3 formation chemistry determines the effect of changes in VOC and NO_x emissions on ozone concentrations.

Various ground-based observation (Nelson et al., 2021; Tan et al., 2018) and model-based methods (Shen et al., 2021; Wang et al., 2019; Wang et al., 2021) have been applied to study O_3-NO_x-VOC sensitivity. The field observation methods can provide accurate in-situ diagnoses of O_3 sensitivity but are limited in temporal and spatial extent (Wang et al., 2017). Air quality model-based methods provide descriptions across time and space. However, uncertainties mainly from emission inventories, as well as meteorological factors and photochemical reactions reduce the accuracy of simulation results (Liu and Shi, 2021). Based on the continuous global observations of formaldehyde (HCHO) and nitrogen dioxide (NO_2) by satellite spectrometers, the space-based HCHO-to-NO_2 ratio can be used as an indicator of O_3 sensitivity because HCHO/NO_2 theoretically reflects the relative availability of NO_x and total organic reactivity to hydroxyl radicals (SILLMAN, 1995). This satellite-based method can provide global-scale photochemical information with good time continuity and little human disturbance, which governments and policymakers are keen to know.

In China, there have been many studies exploring O_3-NO_x-VOCs sensitivity based on satellite-retrieved HCHO/NO_2 (Jin and Holloway, 2015; Li et al., 2021). They are based on thresholds derived from earlier work that used air quality models to link HCHO/NO_2 with surface O_3 sensitivity over the United States (Martin et al., 2004; Duncan et al., 2010; Choi et al., 2012). However, the model approach can be biased because ~~modelled~~ modeled and observed HCHO columns, NO_2 columns, and surface O_3 often disagree. Jin et al. (2020) derived the threshold values from observations and found the transition in O_3 formation regimes occurs at a higher HCHO/NO_2 value than previously determined from models. ~~In addition~~Also, the range of HCHO/NO_2 marking transitional regimes varies regionally because of the differences in meteorological conditions, ozone levels, and precursor composition (Schroeder et al., 2017). The threshold extracted in the United States may not be suitable

55 for China and a uniform value may not be applicable to all Chinese cities. In addition, most previous studies utilized the OMI satellite HCHO/NO$_2$ (Li et al., 2021; Wang et al., 2021). The newly launched TROPOMI aboard Sentinel-5P provides a new perspective to characterize the chemistry of surface O$_3$ at finer spatial scales (Veefkind et al., 2012). Therefore, for a more accurate diagnosis of the ozone-precursor sensitivity across China, Consequently, the transitional regime range of HCHO/NO$_2$ using the new generation of satellites across China requires further in-depth investigationanalysis to diagnose

60 ozone precursor sensitivity..

O$_3$–NO$_x$–VOC sensitivity and changes in VOC and NO$_x$ emissions directly affect ozone concentrations. Nationwide annual estimates of anthropogenic VOC and NO$_x$ emissions in China show different trends from 2013 to 2019, with successive large decreases in NO$_x$ but only slight changes in VOC (Zheng et al., 2018a; Simayi et al., 2022). Previous studies showed that the rapid reduction of NO$_x$ emission increases the surface ozone levels in urban regions (Ren et al., 2021;

65 Yang et al., 2019). In addition, some model simulations suggested that the notable drop of PM$_{2.5}$ is the most crucial factor leading to the O$_3$ increment in China because of the release of HO$_2$ from its uptake on PM$_{2.5}$ (Li et al., 2019). However, this idea remains is highly controversial (Tan et al., 2020). In order to reveal the relationship between ozone increases and changes in its precursors' emissions, satellite-based NO$_2$ and HCHO can be used as visual, timely, and high-resolution trackers of NO$_x$ and VOCs emissions, respectively (Duncan et al., 2010).

70 In this study, we first take advantage of the Chinese extensive air quality monitoring network to assess the latest trends in ozone concentrations comprehensively. The threshold values that mark the O$_3$ formation transition are derived and used to identify the O$_3$–NO$_x$–VOC sensitivity by matching satellite-based HCHO/NO$_2$ with ground-based O$_3$ measurements across China and in different regions. The effects of precursors on ozone and the causes of ozone increase are explored by combining ozone production regimes with interannual variations in NO$_x$ and VOC emissions inferred from tropospheric NO$_2$

75 and HCHO vertical columns. Special measures for plague prevention and work resumption during the COVID-19 pandemic also provide an opportunity to assess O$_3$ response to changes in VOC and NO$_x$ emissions. Furthermore, the optimal VOCs/NO$_x$ reduction ratio is probed in three typical cities, Beijing, Chengdu, and Guangzhou, based on the relationships between O$_3$ and HCHO/NO$_2$, to provide scientific support for future O$_3$ pollution control.

2 Data and Methodology

80 ### 2.1 Ground-Based Observation of O$_3$ and NO$_2$

The Chinese nationwide air quality monitoring network provides surface O$_3$ and NO$_2$ data. Since 2015, more than 1400 sites have covered more than 330 cities across the country. The nationwide hourly O$_3$ and NO$_2$ concentration data in Chinese cities in 2014–2021 were obtained from the National Urban Air Quality Real-Time Publishing Platform (https://air.cnemc.cn:18007/http://106.37.208.233:20035/http://106.37.208.233:20035/).

85 O$_3$ and NO$_2$ measurements were reported in μg m^{-3} and the mass concentrations for all years were unified to the reference state (298.15 K, 1013.25 hPa).O$_3$ and NO$_2$ mass concentrations were reported in μg m^{-3} and unified to the

reference state (298.15 K, 1013.25 hPa). Extensive data quality controls were applied to eliminate unreliable observed outliers following the method of previous studies (Lu et al., 2018). The average of daily NO_2 and the daily maximum eight-hour average (MDA8) O_3 concentration for all national-controlled sites in a city was regarded as the city's daily NO_2 and O_3 levels. The average concentration of all national-controlled sites in a city was regarded as the city's O_3 and NO_2 level.

2.2 Satellite Observations of O_3 Precursors

Given the short lifetime of NO_x, the high NO_2/NO_x ratio in the boundary layer, and the fact that HCHO is an intermediate in the oxidation reactions of various VOCs and is approximately proportional to the total rate of VOC reactions with OH radicals (Duncan et al., 2010), current satellite-based spectrometers have provided continuous global observations for two species indicative of O_3 precursors, namely, NO_2 for NO_X (Lamsal et al., 2014; Martin, 2003) and HCHO for VOCs (Shen et al., 2019; Zhu et al., 2014).

Satellite products of tropospheric NO_2 and HCHO vertical columns are retrieved from two satellite instruments: Ozone Monitoring Instrument (OMI) and Tropospheric Monitoring Instrument (TROPOMI). The high spatial resolution (24×13 km^2 for OMI and 5×3.5 km^2 for TROPOMI) allows for the observation of fine details of atmospheric parameters. They provide daily global observations, and tThe overpass time (13:40–13:50 and 13:30 local time) is well suited to detect the O_3 formation sensitivity when O_3 photochemical production peaks, the boundary layer is high, and the solar zenith angle is small, thereby maximizing instrument sensitivity to HCHO and NO_2 in the lower troposphere (Jin et al., 2017).

The OMI data used for 2013-2020 are developed under the Quality Assurance for Essential Climate Variables (QA4ECV) project. The vertical profiles used for QA4ECV products are obtained from the TM5-MP chemical transport transmission mode model (Williams et al., 2017). The spatial resolutions of OMI NO_2 and OMI HCHO are 0.125° and 0.05°, respectively. The TROPOMI data from the Earth Engine Data Catalog are based on the algorithm developments for the QA4ECV reprocessed dataset for OMI, and have been further optimized. The TROPOMI data, available for 2019-2021, are processed with a spatial resolution of 0.01°. The same chemistry transport model for HCHO and NO_2 is better suited for analysing analyzing their ratio than products developed with different prior profiles.

O_3NO_xOMI data with longer time horizons (2013-2020) are used to study the long-term changes in NO_2 and HCHO through their monthly averages and track changes in emissions of NO_x and VOCs. Since the OMI data retrieved by the QA4ECV project are available until December 2020, the data for 2021 are obtained by converting the TROPOMI data, which is based on a comparison of OMI and TROPOMI monthly data for 2019-2020 to avoid differences in any instrumental offset.

To study the interannual variations in HCHO, NO_2, and HCHO/NO_2, the satellite records are based on TROPOMI observations for the years after 2019 and harmonized OMI observations for 2013-2018. Satellite retrievals must be harmonized to account for differences in any instrumental offset. OMI HCHO and NO_2 data are adjusted with reference to TROPOMI because the latter has a finer spatial resolution and attains a smaller deviation than the former. The instrumental difference between OMI and TROPOMI is estimated as the difference between the two at OMI coarse resolution for the overlapping months. The difference is considered independent of the instrumental

2.3 Connecting Satellite HCHO/NO$_2$ with Ground-Based O$_3$ Observations

125   The high spatial resolution TROPOMI data is used to derive the HCHO/NO$_2$ threshold values marking transitions in O$_3$ formation regimes and to diagnose the current ozone-NO$_x$-VOC sensitivity in China. TROPOMI data are aggregated by sampling gridded NO$_2$ and HCHO columns consistent with the ground-based observations of O$_3$. O$_3$ concentrations are averaged at all available sites every half month for the warm season (April to September) from 2019 to 2021. O$_3$ measurements at 13:00 to 14:00 local time are selected to match the TROPOMI overpass time. Considering the data

130   volume and the need to reduce retrieval noise, TROPOMI-retrieved NO$_2$ and HCHO columns are sampled every half month over O$_3$ sites for the same period, yielding nearly 100 000 paired observations. In addition, considering the amount of available data and topographic conditions, China is divided into nine regions to evaluate the satellite-based HCHO/NO$_2$ and study the O$_3$ production regimes, as shown in Fig. S2. Based on satellite and surface observations, the response of O$_3$ concentrations and changes in O$_3$ precursors are compared in two typical cities, Beijing and Chengdu, during the plague

135   prevention of COVID-19 pandemic and the work resumption COVID-19 pandemic in spring 2020 to assess the effectiveness of the O$_3$ production regimes for satellite HCHO/NO$_2$ capture.

3 Results and Discussion

3.1 Surface Ozone Trends

    The ozone concentrations averaged from 367 cities with monitoring sites in China from 2015 to 2021 are shown in Fig.

140   1a. The three metrics include the maximum 6-month MDA8 ozone running average (MMA6-MDA8) and the 90th and 99th percentiles of the annual distribution of MDA8-O$_3$ (MDA8-90th, MDA8-99th), following the definition in World Health Organization global air quality guidelines (World Health Organization, 2021) and Chinese ambient air quality standards (GB 3095-2012). The three metrics increased at 2.3 (2%), 2.5 (2%), and 2.3 (1%) μg m^{-3} year^{-1} in 2015-2021. Moreover, they significantly increased at 4.6 (5%), 5.6 (4%), and 5.4 (3%) μg m^{-3} year^{-1} (all with $p < 0.05$) in 2015-2019, based on the

145   linear trend estimate.

5
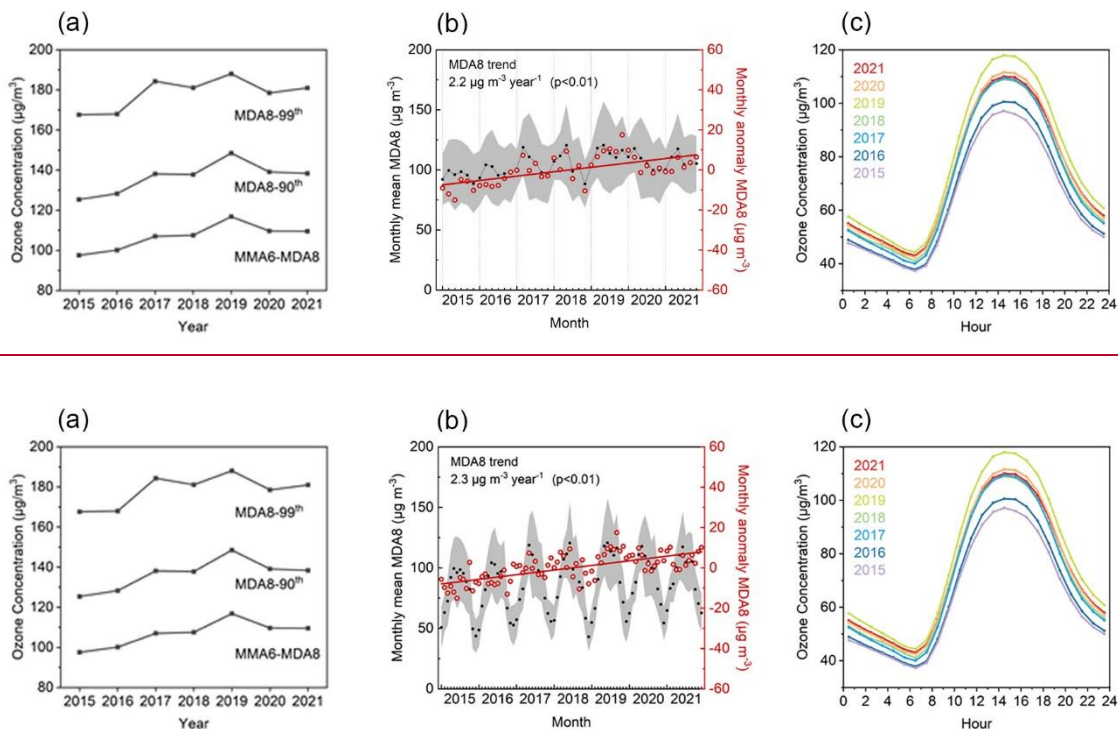
Figure 1: Surface ozone concentrations in China. (a) MDA8-99th, MDA8-90th, MMA6-MDA8, and (b) monthly average (black dots, left axis) and anomaly (circle, right axis) of MDA8 ozone concentrations averaged from all 367 cities with monitoring sites in 2015–2021. Gray shading: mean value ± standard deviation across all cities for each month. Solid line: linear fitted curve. (c) Ozone diurnal cycles from April to September.

The time series of the monthly mean MDA8 ozone in 2015–2021 is shown in Fig. 1b. Based on the monthly anomalies (the difference between the observed monthly mean and the 7-year monthly mean for the same month), MDA8 ozone levels increased by 2.3 μg m^{-3} year^{-1} (3.0% year^{-1}, $p < 0.01$) averaged from all cities. The increases are also exhibited rapidly before 2019, with 3.5 μg m^{-3} year^{-1} (4.5% year^{-1}, $p < 0.01$). The daytime and nighttime mean ozone levels show similar trends. In 2015–2019, the maximum and minimum hourly average concentration increased from 97.1 to 117.9 μg m^{-3} and from 37.3 to 44.3 μg m^{-3}, respectively, based on the mean April to September ozone diurnal variation, as shown in Fig. 1c. Overall, the average ozone concentration shows an increasing trend from 2015 to 2021, although it has decreased in the last two years compared to the peak in 2019.

6

(a) MDA8-90 (μg m⁻³)

(b) MDA8-90 trend (μg m⁻³ yr⁻¹)
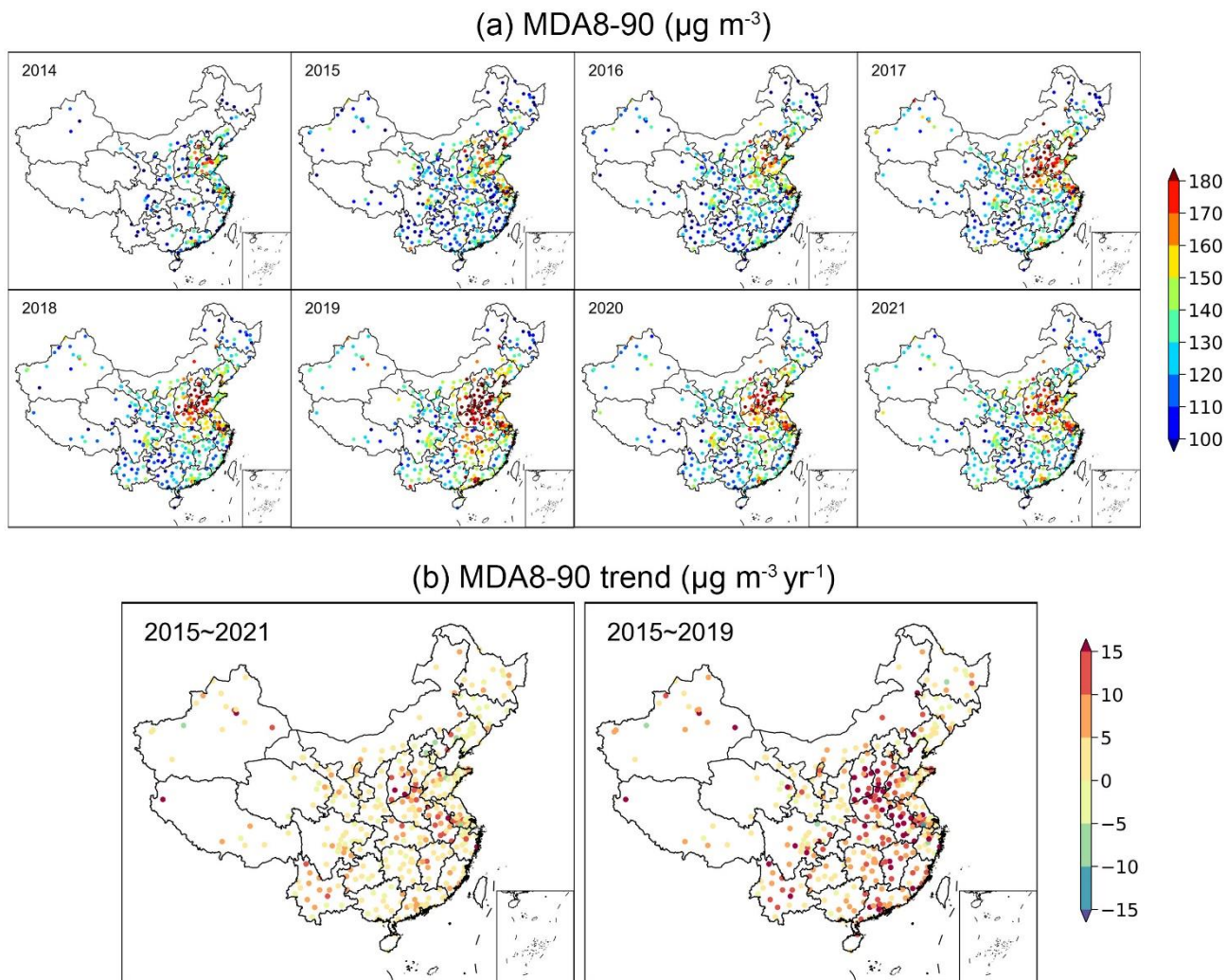
160

Figure 2: Spatiotemporal distributions of MDA8-90th ozone in China from 2014 to 2021, and trends for 2015–2019 and 2015–2021.

The spatial patterns of MDA8-90th and their trends for approximately 367 cities in 2014–2021 are shown in Fig. 2. The cities with high ozone levels are widely distributed in eastern and central China, where intensive anthropogenic emissions are located. Distinct exacerbation of ozone pollution can be observed from 2014 to 2019. The locations and definitions of the key regions are shown in Fig. S1. In 2014–2015, sites with MDA8-90th greater than 160 μg m⁻³ were concentrated near the Beijing-Tianjin-Hebei and the Yangtze River Delta (YRD) megacity clusters. By 2019, ozone hot spots extended westward to the Fenwei Plain and southward to the central Yangtze River Plain. During the 6 years, the ozone concentration has increased almost everywhere in China, particularly in the North China Plain (NCP) and the central Yangtze River Plain. In 2020 and 2021, ozone pollution was alleviated; the level of which is equivalent to the level of ozone pollution in 2017–2018.

O$_3$ concentration decreases in major key regions, including the North China Plain, Pearl River Delta (PRD), and Sichuan Basin (SCB).

The percentage of sites with MDA8-90th ozone higher than 160 μg m^{-3}, the Chinese grade II national air quality standard, increased from 15.0% in 2015 to 39.3% in 2019 and then decreased to 23.0% in 2021. The percentage of sites with increasing ozone trends was 83.1% in 2015–2019 and 71.8% in 2015–2021. From a national perspective, widespread surface ozone increases occurred in Chinese cities during 2015–2019. Moreover, decreases have been observed in the last 2 years.

3.2. Ozone–NO$_x$–VOC sensitivity over China

3.2.1 Ozone–NO$_x$–VOC Chemistry Captured by Satellite-Based HCHO/NO$_2$

Ozone formation can be limited by NO$_x$, VOCs, or both. Satellite-based HCHO and NO$_2$ columns are evaluated whether they can capture the nonlinearities in O$_3$–VOCs–NO$_x$ chemistry. Figure 3a, similar to classic ozone isopleths typically generated with models (Sillman et al., 1990; Pusede et al., 2015), shows the in situ O$_3$ concentration as a function of TROPOMI NO$_2$ and HCHO derived solely from observations.
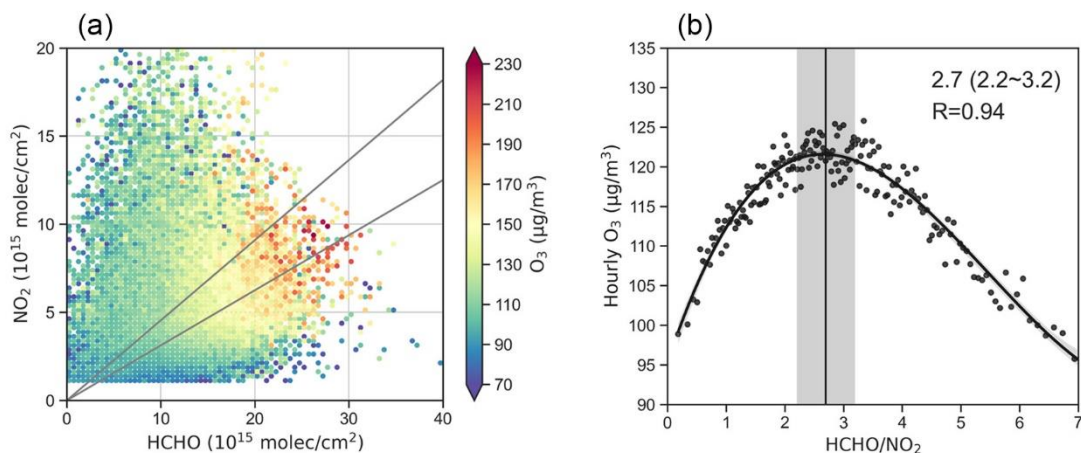
Figure 3: (a) O$_3$ concentration as a function of TROPOMI HCHO and NO$_2$. All surface hourly O$_3$ observations (13:00 to 14:00 local time) averaged over each half month from April to September 2019–2021 are aggregated based on the corresponding TROPOMI HCHO and NO$_2$ (interval: 0.5 unit × 0.25 unit). The black lines delineate the TROPOMI HCHO/NO$_2$ values of 2.2 and 3.2. (b) O$_3$ concentration (13:00 to 14:00) as a function of TROPOMI HCHO/NO$_2$. O$_3$ average concentration is calculated by first matching hourly O$_3$ observations with TROPOMI HCHO/NO$_2$ for each half of the month, dividing these paired observations into 200 bins based on HCHO/NO$_2$, and then calculating the O$_3$ average concentration (y axis) for each TROPOMI HCHO/NO$_2$ bin (x axis). The solid line is fitted with third-order polynomial curves, and the shading indicates 95% confidence intervals. The vertical lines indicate the maximum of the fitted curve, and the vertical shading represents the range with the curve slope from −3 to +3 (regime transition).

Consistent with O$_3$ isopleths, O$_3$ concentration is a non-linear process in relation to NO$_2$ and HCHO, as shown in Fig. 3a. Three regimes can be roughly identified. When HCHO is low and NO$_2$ is relatively high, the O$_3$ concentration is high at lower NO$_2$ or higher HCHO, indicating VOC-limited (or NO$_x$-saturated) chemistry. When NO$_2$ is low and HCHO is relatively high, the O$_3$ concentration increases with increasing NO$_2$, indicating NO$_x$-limited chemistry. When both NO$_2$ and

8

HCHO are high, O_3 concentration peaks and increases with both increasing NO_2 and HCHO. However, the division between the three regimes is uncertain and ambiguous, which may be influenced by other factors such as different meteorology, noisy satellite retrievals, the spatial mismatch between gridded satellite observations and point measurements on the ground, and lack of statistical power to calculate average concentrations in some intervals due to small sample sizes. Despite these uncertainties, Figure 3a qualitatively illustrates the nonlinear relationship between O_3 and satellite NO_2 and HCHO, similar to the overall O_3-NO_x-VOC chemistry.

After the qualitative approach is established, the HCHO/NO_2 thresholds that mark the O_3 transitional regime are then derived by calculating the average ozone concentration for a given TROPOMI HCHO/NO_2 from Fig. 3a and examining their statistical relationships in China and the different regions within it. Empirical relationships are investigated by applying second-order and third-order polynomial models (Jin et al., 2020) to the observations over all cities in China. The third-order polynomial model is used to derive the maximum mean O_3 concentration (the peak of the curve in Fig. 3b) because it fits the data with the high correlation coefficient better than the second-order model does. Assuming that the peak of the curve (with a slope of 0) marks the transition from VOC-limited to NO_x-limited regimes (Pusede and Cohen, 2012), the transitional regime (mixed sensitive regime) is defined as the range with a slope between −3 and +3.

The aggregation of the overall available observations used in Fig. 3a shows that the O_3 concentration peaks at HCHO/NO_2 are equal to 2.7, with the transitional regime between 2.2 and 3.2. A separate evaluation for nine regions also reveals the strong nonlinear relationships between the O_3 concentration and TROPOMI HCHO/NO_2, despite differences in the overall O_3 concentrations. The Pearson correlation coefficient between the fitted third-order polynomial curve and the data is generally more than 0.73, except for Inner Mongolia (0.59). The HCHO/NO_2 marking the regime transition varies among these regions (Table 1 and Fig. S3), with the highest in Shanxi-Shaanxi-Henan [3.7 (3.2–1.3)] and the lowest in Heilongjiang-Jilin-Liaoning [2.0 (1.2–3.2)]. Different cities respond differently to changes in NO_x and VOC emissions. Previous studies have also demonstrated regional differences in the threshold values of HCHO/NO_2 (Schroeder et al., 2017; Chang et al., 2016) and other photochemical indicators (Liu and Shi, 2021). This difference among regions may reflect environmental conditions (Liu and Shi, 2021), such as radiation intensity and surface temperature. This varied response is also reflected in different thresholds for other photochemical indicators (Liu and Shi, 2021; Wang et al., 2017) or patterns of O_3 isopleths (Shen et al., 2021). This difference among regions may reflect environmental conditions (Liu and Shi, 2021), such as radiation intensity and surface temperature.

Table 1. HCHO/NO₂ threshold values between O₃ production regimes in nine Chinese regions

Region	Correlation coefficient [a]	HCHO/NO₂ [b]	Transitional regime
Beijing-Tianjin-Hebei-Shandong	0.93	3.4	3.0–3.8
Shanxi-Shaanxi-Henan	0.93	3.7	3.2–4.3
Shanghai- Jiangsu-Zhejiang-Anhui	0.85	2.7	2.2–3.3
Jiangxi-Hubei-Hunan-Fujian	0.76	3.2	2.2–4.7
Guangdong-Hong Kong-Macao- Guangxi-Hainan	0.82	3.2	2.7–3.8
Sichuan-Chongqing- Guizhou-Yunnan	0.73	3.2	2.5–4.3
Gansu-Ningxia-Qinghai-Tibet-Xinjiang	0.74	3.0	2.2–4.5
Inner Mongolia	0.59	2.5	1.9–3.4
Heilongjiang-Jilin-Liaoning	0.82	2.0	1.2–3.2

[a] The Pearson correlation coefficient between the fitted third-order polynomial curve and the data.

225   [b] HCHO/NO₂ value at the maximum of the fitted curve (peak O₃ concentration).

The HCHO/NO₂ thresholds in the present study are higher than the previously reported model-based values, such as 1~2 by Jin and Holloway (2015) and Duncan et al. (2010), and 1.5~2.3 by Chang et al. (2016). Thus, this observation-based method indicates that O₃ production tends to be VOC limited at the same HCHO/NO₂. This discrepancy stems from the different approaches linking HCHO/NO₂ to O₃ production regimes. Previous modelling studies derived thresholds by

230   simulating the response of surface O₃ to the overall reductions in NOₓ or VOC emissions. Moreover, these thresholds were derived from the study area in the United States, which best represents regional rather than local O₃-NOₓ-VOC sensitivities (Martin et al., 2004; Jin et al., 2017). Thresholds derived with in situ observations in China take full account of the local O₃ chemistry.

3.2.2 Spatial Distribution of O₃ Production Regimes

235   The derived HCHO/NO₂ thresholds were used to identify the O₃ production regimes over China from April to September 2019 3–2021. Based on the same HCHO/NO₂ threshold across China (2.2–3.2, Fig. S3) and different thresholds for different regions (Fig. 4 and S4), two methods yield similar spatial distributions of O₃ sensitivity (Fig. S4 and 4). However, the regional approach suggests that O₃ production tends to be VOC limited because the HCHO/NO₂ thresholds derived in many key regions individually are higher than the national overall threshold.
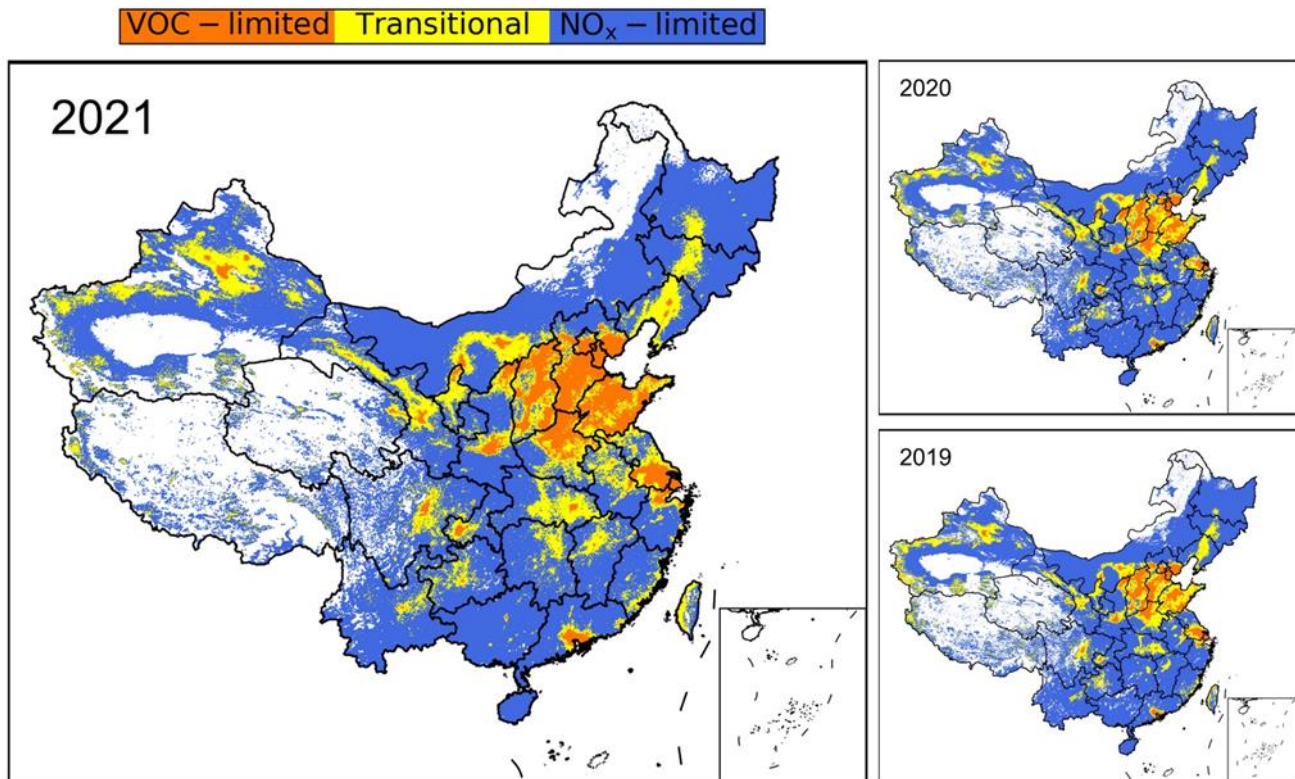
10

240

11
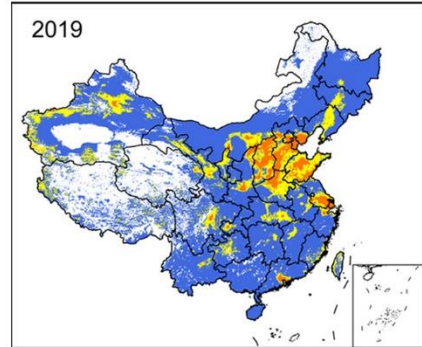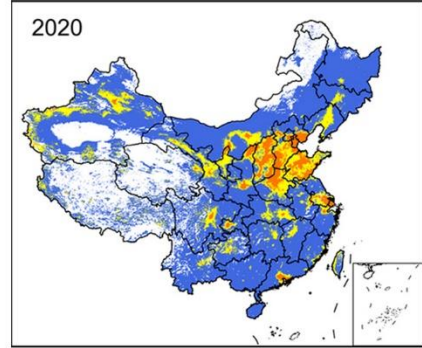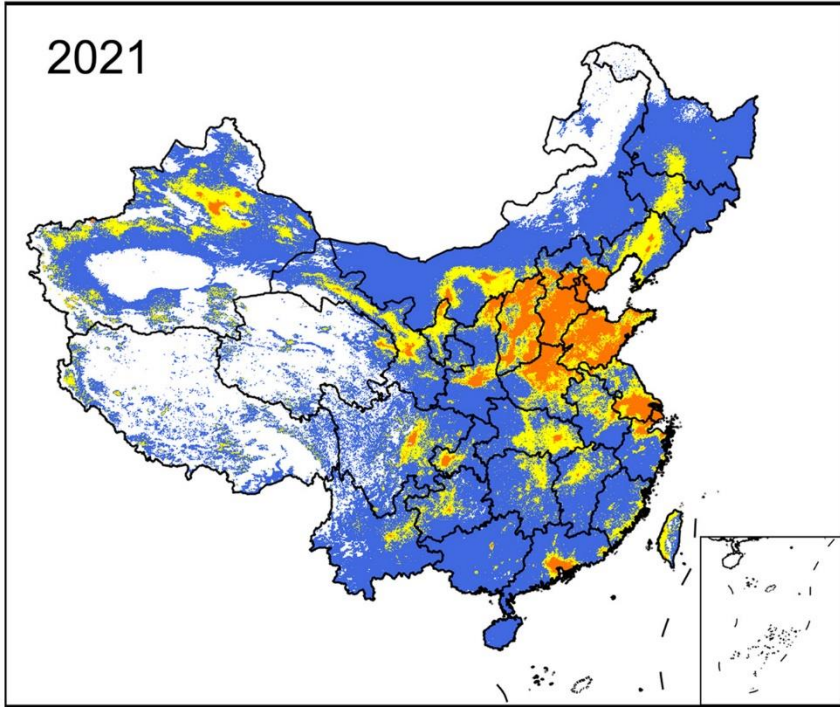
Figure 4: Ozone sensitivity classification over China from April to September ~~2013, 2015, 2017 and~~ 2019–2021 using different HCHO/NO₂ thresholds in different regions. Only polluted regions are displayed (defined as average TROPOMI NO₂ columns higher than 1.0×10^{15} molecules/cm²).

245   As shown in Fig. 4, the NO$_x$-limited regime dominates in most regions from April to September. VOC-limited chemistry exists in urban areas of almost every province, with transitional regimes occurring around the VOC-limited regimes in wide urban and suburban areas. Widespread VOC-limited and transitional regimes are observed over major megacity clusters. In the North China Plain, the VOC-limited regimes are distributed in Beijing and most regions in the provinces of Hebei, Shanxi, Henan, and Shandong. Transitional regimes control almost all the remaining regions, except for

250   individual cities in northern Hebei and southwestern Henan. The percentages of VOC sensitive regime and the transitional regime are 59.2% and 26.7% in 2021 (Table S1). In the Yangtze River Delta, the VOC-limited regimes are found in some developed urban cities including Shanghai, some cities in southern Jiangsu Province (such as Suzhou, Wuxi, and most of Nanjing and Nantong) and Zhejiang Province (Jiaxing, urban of Hangzhou and Ningbo). VOC-limited and transitional or mixed regimes occupy 23.5% and 31.4% of the total grid cells (Table S1). In the Pearl River Delta and surrounding areas

255   (Guangdong Province), VOC-limited regimes (8.0%) and transitional regimes (11.0%) control Shenzhen, Dongguan, Foshan, Zhongshan, Zhuhai, most of Guangzhou, and some other urban areas, whereas NO$_x$-sensitive regimes dominate most of the remaining cities. In addition, extensive VOC-limited and transitional regimes occur in developed cities of Sichuan Basin (urban centres of Chongqing and Chengdu), Shaanxi Province (Xi'an), Hubei Province (Wuhan), and other regions.

12

Compared with previous studies (Jin and Holloway, 2015; Wang et al., 2019), the results of this study are slightly different. The areas dominated by VOC-limited and transitional regimes in China are expanded, especially in NCP; while in the southern region (e.g., Guangdong Province), VOC-sensitive regimes are only concentrated in major cities.

Air quality monitoring sites are generally located in built-up areas of cities, representing the environment in which people live. The ozone sensitivity regime of all monitoring sites' locations based on $HCHO/NO_2$ and the O_3 MDA8-90th in 2021 are shown in Fig. S5. VOC-limited and transitional regimes dominate O_3 formation at 86.2% of the sites, with VOC-limited chemistry accounting for 52.5%.

The comparison of O_3 sensitivities from 2019~~3~~ to 2021 (Fig. 4 ~~and S4~~) shows a slight change in the trends of individual regions from VOC-limited regimes to transitional regimes or from transitional regimes to NO_x-limited regimes as a result of NO_x reduction. However, there has been no remarkable change in China as a whole. The changes in VOC and NO_x emissions in recent years have not led to the transition in the spatial distribution of the O_3 production regime defined by our $HCHO/NO_2$ thresholds.

3.3 ~~Effects of Interannual Variations in Ozone Precursors~~Effects of Ozone Precursors Variations on Ozone
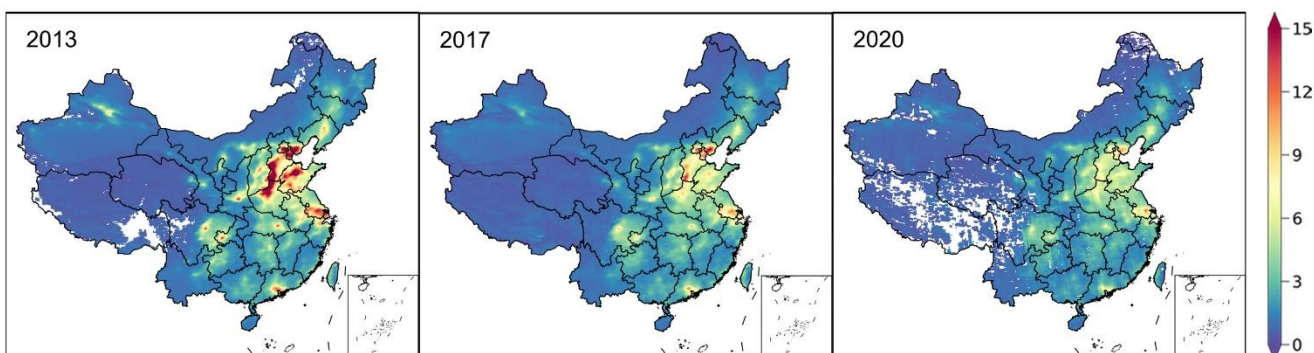
3.3.1 Interannual Variations in Ozone Precursors

Based on the non-linear O_3-NO_x-VOC relationship, changes in ozone precursors can directly affect ozone levels.~~Based on the non-linear relationship of O_3-NOx-VOC, the changes in ozone precursors is the direct factor affecting ozone level.~~ Ground-based measurements of NO_2 and satellite-based NO_2 columns are used to indicate the changes in NO_x emissions. As shown in Fig. 5a and S6, NO_2 is concentrated over urban areas and industrial cities, particularly in megacity clusters, such as the NCP, YRD, and PRD, and large cities, such as Wuhan (in Hubei) and Xi'an (in Shaanxi). Satellite observations show large NO_2 decreases from 2013. This finding is consistent with previous studies (Wang et al., 2019; Lin et al., 2019). Moreover, the decrease is more than 2.8% per year in half of the grids. Figure 5b shows that the average annual reduction in satellite NO_2 in eastern China is 3.7% (0.18×10^{15} molecules cm^{-2}, $p < 0.01$). A reverse increase has occurred in the last 2 years, mainly in winter. Figure S8~~7~~ shows similar trends in surface NO_2 concentrations and satellite-based NO_2 columns averaged in April–September ~~from 2015 to 2021~~. More than 75% of the cities show negative trends in surface NO_2 levels (and 22% with $p < 0.05$), and nearly 73% of the grids show decreases in satellite NO_2 columns. Strong and consistent decreases in high-value areas, particularly the NCP, as well as YRD, PRD, and SCB, have been observed in the last 9 years. The mean NO_2 in NCP has decreased by 0.59×10^{15} molecules cm^{-2} $year^{-1}$ (5.0%, $p < 0.01$) from 2013 to 2021.

The variations in ~~anthropogenic~~ VOCs primarily drive the temporal patterns of satellite HCHO columns over China (Shen et al., 2019). The changes in satellite HCHO can roughly indicate changes in VOC emissions, which has been applied in several previous studies (Li et al., 2020; Shen et al., 2019; Zhu et al., 2014). Figures 6a and S7~~6~~ compare the HCHO columns from April to September 2013–2021. As expected, a clear gap exists between the HCHO in southeast and northwest China. The mean HCHO is high over megacity clusters in the southeastern regions, such as the Northern China Plain,
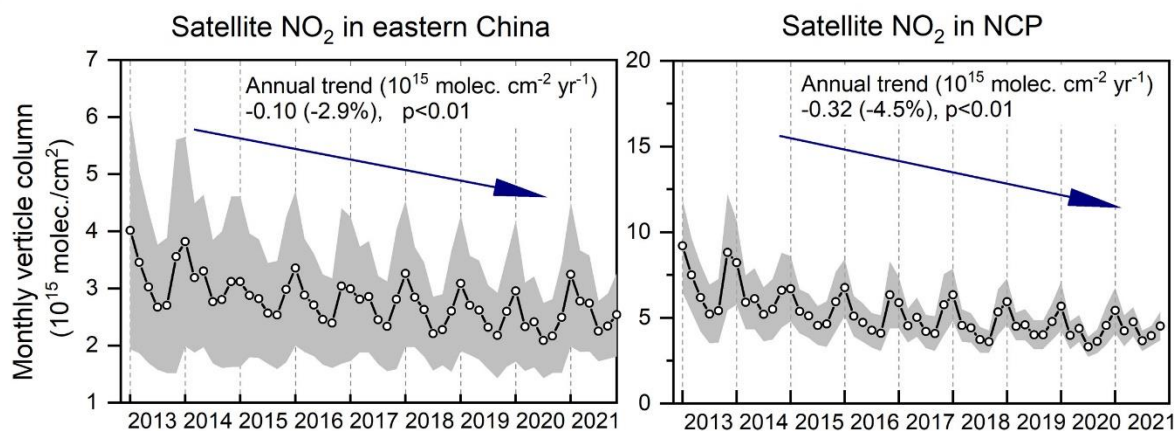
Sichuan Basin, Yangtze River Delta, Pearl River Delta, and the Central Yangtze River Plain. More than 45% of the grids show positive trends in satellite HCHO columns in 2013–2021. HCHO columns increase by 0.01% year^{-1}, averaged from all grids in 2013–2021 in eastern China. This finding is consistent with the increases in anthropogenic VOC emissions (Zheng et al., 2018b; Zhang et al., 2019). In 2020–2021, satellite-based HCHO decrease in most of eastern China compared to 2019.

295   In addition to anthropogenic and biogenic emissions, Tthe long-term changes in HCHO are driven by several other factors (Zhu et al., 2017): NO$_x$ reductions can lower the HCHO yield from isoprene oxidation (Souri et al., 2020; Wolfe et al., 2016), and in addition, HCHO columns may show interannual variability driven by interannual variability of meteorology, particularly temperature as shown in Fig. S9 (Duncan et al., 2009; Abbot et al., 2003). Nevertheless, HCHO has not declined as dramatically as NO$_2$, particularly until 2019. In the NCP, where VOC-limited chemistry most widely exists, the gap

300   between HCHO and NO$_2$ changes is even larger.

(a) Satellite NO$_2$ (molec/cm^2)

(b)

Satellite NO$_2$ in eastern China

Annual trend (10^{15} molec. cm^{-2} yr^{-1})
-0.10 (-2.9%),   p<0.01

Satellite NO$_2$ in NCP

Annual trend (10^{15} molec. cm^{-2} yr^{-1})
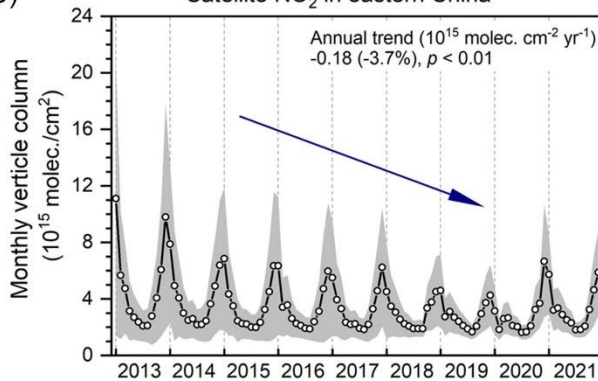-0.32 (-4.5%),   p<0.01

~~Figures 6a and S6 compare the HCHO columns from April to September 2013–2021. As expected, a clear gap exists between the HCHO in southeast and northwest China. The mean HCHO is high over megacity clusters in the southeastern regions, such as the Northern China Plain, Sichuan Basin, Yangtze River Delta, Pearl River Delta, and the Central Yangtze River Plain. More than 45%~~

14

305 ~~of the grids show positive trends in satellite HCHO columns in 2013–2021. HCHO columns increase by 0.01% year^{-1}, averaged from all grids in 2013–2021 in eastern China. This finding is consistent with the increases in anthropogenic VOC emissions~~ **(Zheng et al., 2018b; Zhang et al., 2019)** ~~. In 2020–2021, satellite-based HCHO decrease in most of eastern China compared to 2019. The changes in HCHO are driven by several factors~~ **(Zhu et al., 2017)** ~~: NOx reductions can lower the HCHO yield from isoprene oxidation~~ **(Souri et al., 2020; Wolfe et al., 2016)** ~~, and in addition, HCHO columns may show interannual variability driven by~~

310 ~~interannual variability of meteorology, particularly temperature~~ **(Duncan et al., 2009; Abbot et al., 2003)** ~~. Nevertheless, HCHO has not declined as dramatically as NO$_2$, particularly until 2019. In the NCP, where VOC-limited chemistry most widely exists, the gap between HCHO and NO$_2$ changes is even larger.~~
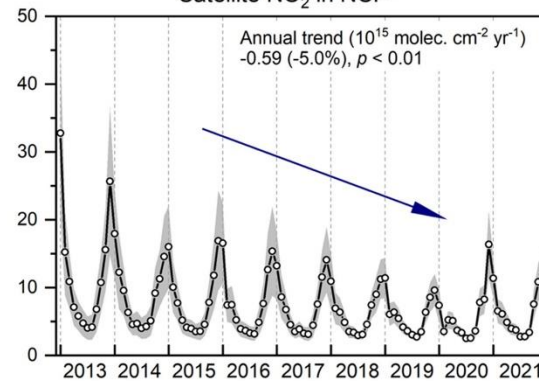
(a) Satellite NO$_2$ (molec/cm^2)

(b)
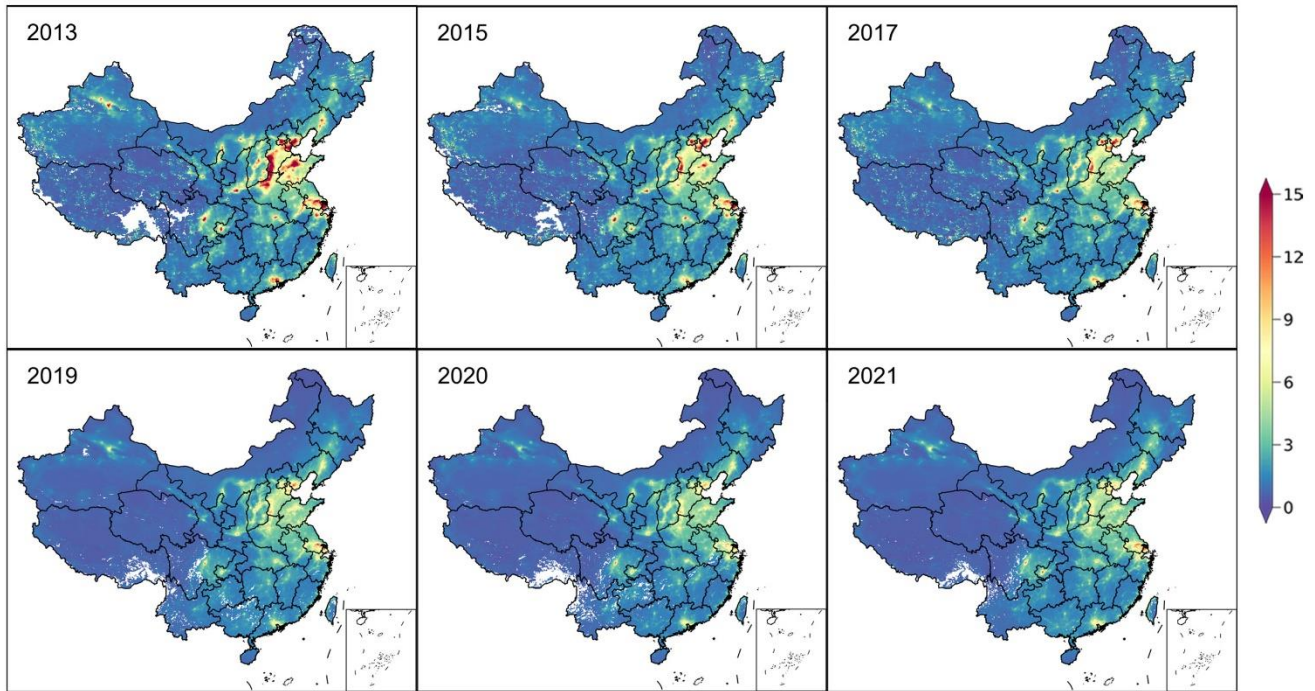
Figure 5: (a) Maps of average satellite-based NO$_2$ columns over China from April to September, and (b) monthly mean NO2 columns averaged over eastern China and North China Plain in April-September. Gray shading: mean value ± 50% standard deviation across all grids for each month. Solid line: the linear fitted curve. Inset: absolute annual linear trend and percentage of annual trend (% per year, the linear trend divided by the 2013 mean values).

(a) Satellite HCHO (molec/cm^2)

(b)

Satellite HCHO in eastern China

Annual trend: (10^{15} molec. cm^{-2} yr^{-1})
-0.02 (-0.1%)

Monthly verticle column (10^{15} molec./cm^2)

Satellite HCHO in NCP

Annual trend: (10^{15} molec. cm^{-2} yr^{-1})
-0.02 (-0.2%)
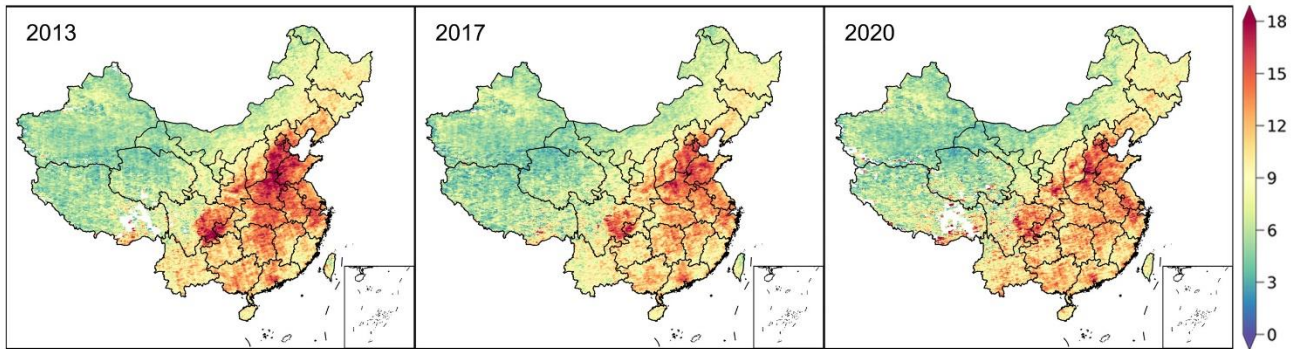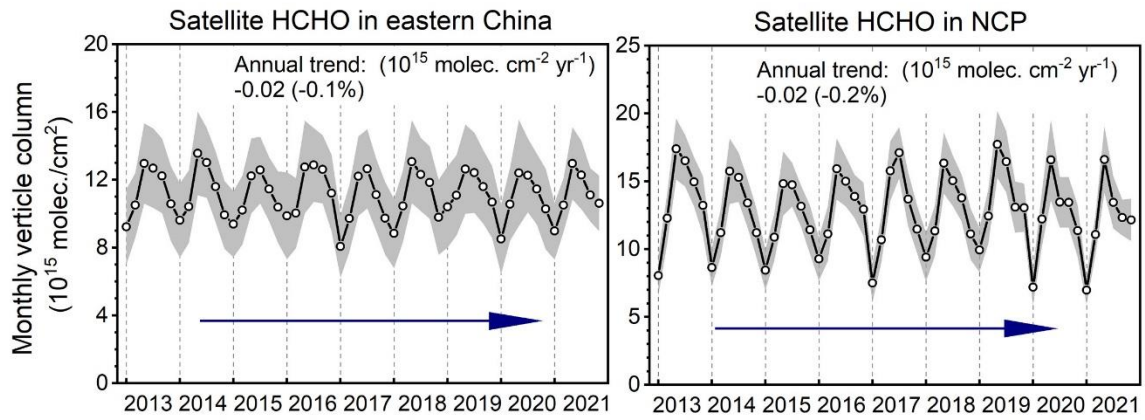
(a) Satellite HCHO (molec/cm²)
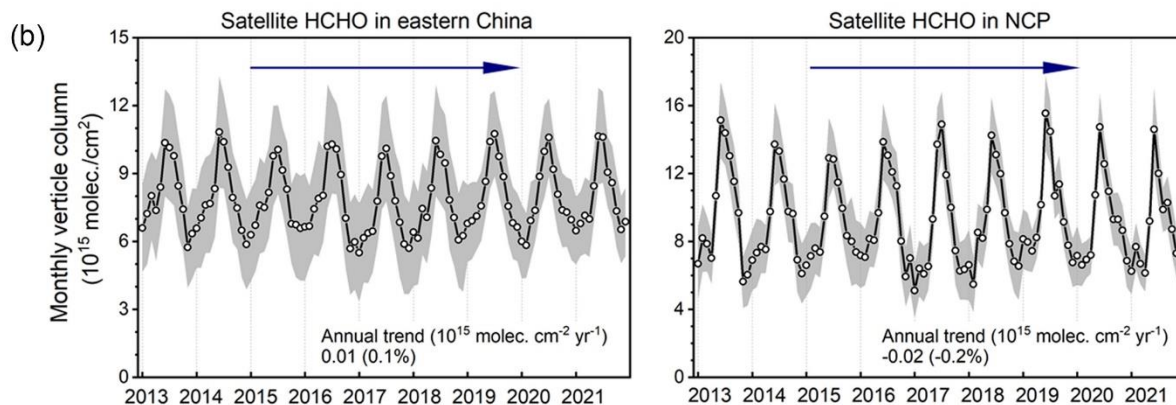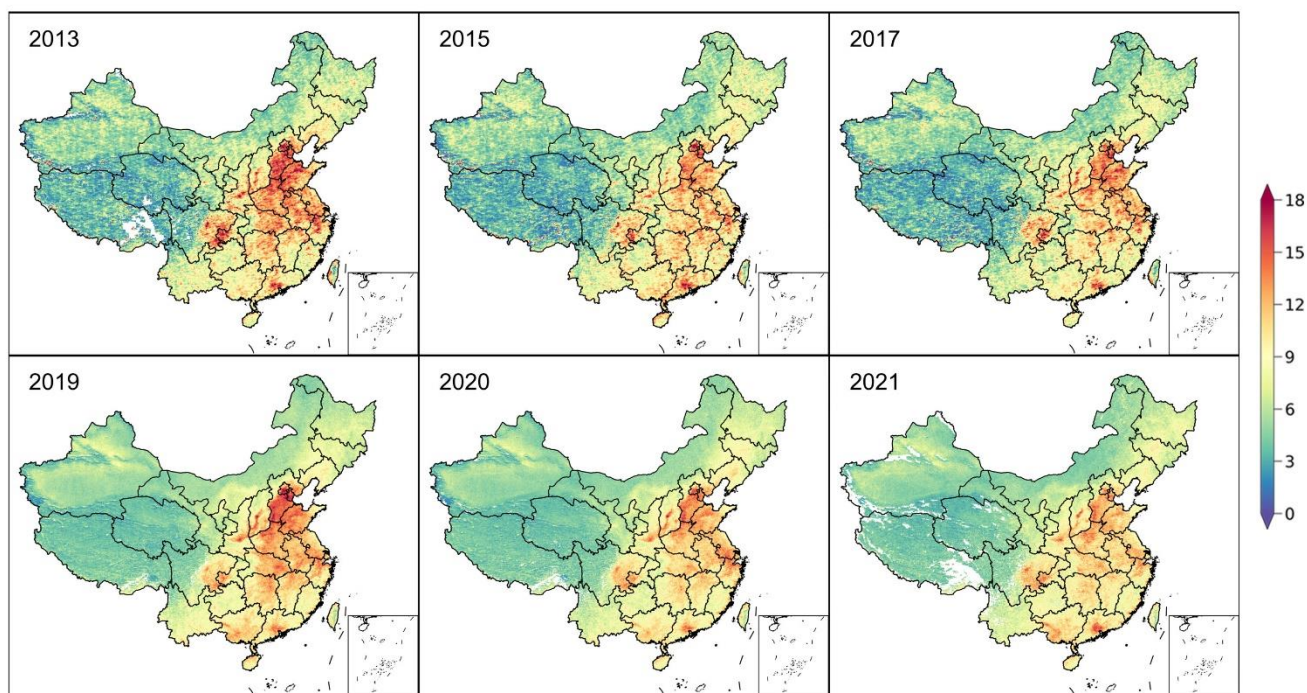
Figure 6: Same as Figure 5 but for satellite-based HCHO columns.

The changes in VOC and NO_x emissions presumably have the same disparity as the changes in satellite HCHO and NO_2. The anthropogenic NO_x emission has been decreased considerably since 2013. However, VOC emissions have not been effectively reduced or even slightly increased. The significant NO_x reduction alone without effective VOC control has not worked or has even aggravated O_3 pollution in recent years because of the VOC-limited (or NO_x-saturated)

18

325   O$_3$ production regimes in major city clusters. ~~Considering that biological VOC also increased~~ (Li et al., 2020), it is clear that the reduction of anthropogenic VOCs is not sufficient to bring down the total VOC emissions.

3.~~3.2~~4 Cases of O$_3$ responses to the changes in its precursors

    The outbreak of the COVID-19 pandemic produced previously unseen societal impacts in China. ~~Compared to normal years,~~ Tthe measures during the plague prevention and the work resumption resulted in changes in VOC and NO$_x$ emissions

330   in 2020 compared to normal years (Le et al., 2020; Pei et al., 2022), ~~.~~ and these ~~The~~ changes ~~, which~~ ~~were~~are not ~~uniform or~~ synchronized across Chinese cities.~~across the country,~~ The ozone pollution that occurred in Beijing and Chengdu during this period is used as natural experiments ~~serve as a natural experiment~~ to evaluate surface O$_3$ responses to ~~a~~ apparent ~~marked~~ emission variations in order to validate the conclusions above. ~~.~~

    In Beijing, the capital of China, the average O$_3$ MDA8 concentration reached 118.9 µg m^{-3} in April 2020, which is 15.5%

335   and 11.9% higher than that in April 2019 and 2021 (Fig. 7a). The satellite or ground-based observations of NO$_2$ and HCHO show variations in NO$_x$ and VOCs. NO$_2$ concentrations were the lowest in April 2020 compared with the monthly means in April 2019 and 2021, showing reductions of 33.2%–42.1% and 17.8%–28.5%. This scenario is associated with a massive reduction in human activity (Le et al., 2020). Unlike the change in NO$_2$, HCHO columns in April 2020 are only 16.5% lower than those in 2019 and even 8.7% higher than those in 2021. In the NO$_x$-saturated (VOC-limited) regime, VOC emission

340   reductions are generally effective in reducing O$_3$ concentrations. However, the former is primarily offset by the reduction in NO$_x$ emissions resulting in a low titration of O$_3$ by NO$_x$, causing directly the increase in O$_3$~~which directly increases O$_3$~~ ~~combined with the relatively high temperature and low humidity~~.
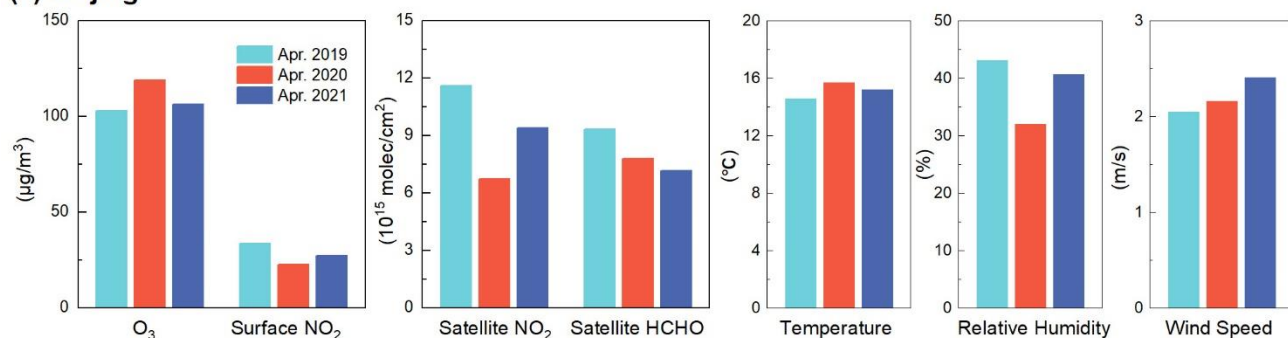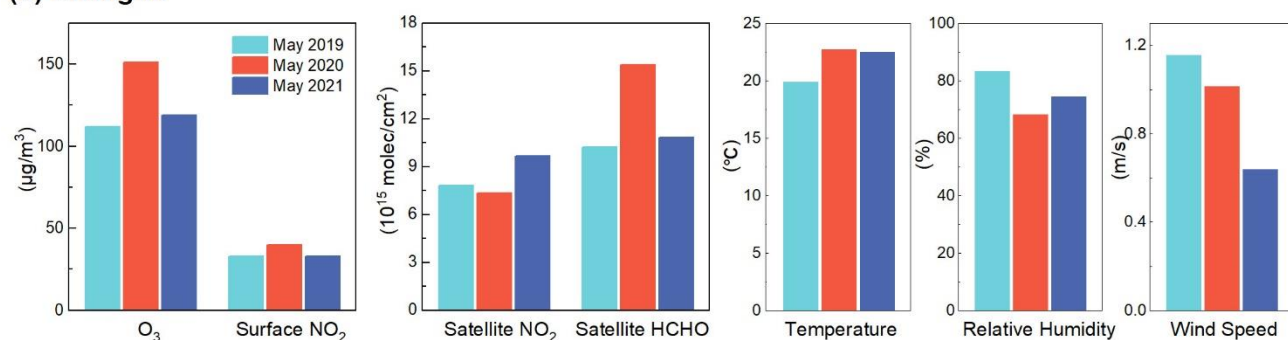
Figure 7: Ground-based observation of O₃ and NO₂, satellite-based NO₂ and HCHO, and meteorological conditions, including temperature, relative humidity and windspeed in (a) Beijing and (b) Chengdu, Sichuan. The figure compares monthly averages for Beijing in April and for Chengdu in May 2019–2021.

~~Serious~~Severe ozone pollution occurred in Chengdu, the capital of Sichuan Province, in May 2020, with the maximum hourly ozone concentration reaching 258.8 µg m^{-3}. The monthly average MDA8 is 34.8% and 26.9% higher than that in May 2019 and 2021, respectively. Compared with the monthly means in May 2019 and 2021, the monthly means in May 2020 demonstrate the almost constant NO₂ (−6.1% to 21.2% and −24.3% to 21.2%) and the considerable increase in HCHO (50.7% and 42.2%), as shown in Fig. 7b, which is associated with the increase in VOC emissions (Song et al., 2022). As expected, the increase in VOC emissions is a major contributor to the growth of O₃ because of the VOC-limited conditions in Chengdu. At that time, after the strictest restrictions, Chengdu was vigorously developing the stall business to help work resumption. The increase in VOCs may be related to open-air cooking emissions (Liang et al., 2022).

~~This scenario may be related to the vigorous development of stall businesses in Chengdu at that time to help work resumption.~~ In these two cases in Beijing and Chengdu, meteorological conditions also contributed to the increase in ozone concentrations. As shown in Figure 7, compared to the previous and subsequent years, there is only a slight increase in temperature; relative humidity decreases, but remains high in Chengdu (over 60%); wind speed is not the lowest in the three years. Although the effects of emissions and meteorological conditions are difficult to distinguish quantitatively, it reflects the negative effect of NO$_x$ reduction alone or VOC increase on O₃ pollution in urban cities.

~~These two cases in Beijing and Chengdu verify the negative effect of NOx reduction alone or VOC increase on O₃ pollution in urban cities.~~ **3.4 VOC/NO$_x$ Reduction Ratio for Typical Cities**

The synergistic control of NOx and VOC, with VOC control as the focus, can help reduce ozone pollution in major cities. The reduction ratio of VOC/NO$_x$ can be indicated by the slope of the ridge line of the classic ozone isopleths (Ou et al., 2016; Wang et al., 2019). The relationship between O$_3$ concentrations and the satellite HCHO and NO$_2$ columns reflected by the approach in Figure 3a is similar to the O$_3$-VOC-NO$_x$ isopleths. Thus ~~Based on the method in Fig. 3, O₃ concentrations and the satellite HCHO and NO₂ relationships similar to the O₃ isopleths are obtained. The~~ the peak of the fitted curve of O$_3$ and HCHO/NO$_2$, corresponding to the ridge line of O$_3$ isopleths, ~~HCHO/NO₂ value at the peak of the fitted curve~~ is the ratio of HCHO to NO$_2$ reduction for the fastest decrease in O$_3$, ~~concentration~~ i.e., ΔHCHO/ΔNO$_2$.

This approach is used to provide preliminary scenarios for synergistic VOC and NO$_x$ reduction in ~~T~~three ~~typical~~ developed cities, ~~namely,~~ Beijing in the NCP, Guangzhou in the PRD, and Chengdu in the SCB, which are all dominated by the VOC-limited regime. ~~, are selected to study the reduction pathways, a~~As shown in Fig. 8, ~~t~~The optimal decrease ratio of HCHO to NO$_2$ is between 2:1 and 4:1, which is 3.4–3.9 for Beijing, 2.2–2.6 for Chengdu, and 2.3–2.8 for Guangzhou. The results obtained by this method roughly reflect the optimal abatement pathways for the two precursors by using the satellite HCHO and NO$_2$ to represent VOC and NO$_x$. The short-term future O$_3$ control becomes much more promising in terms of enhanced VOC control in urban cities dominated by VOC-limited regimes.
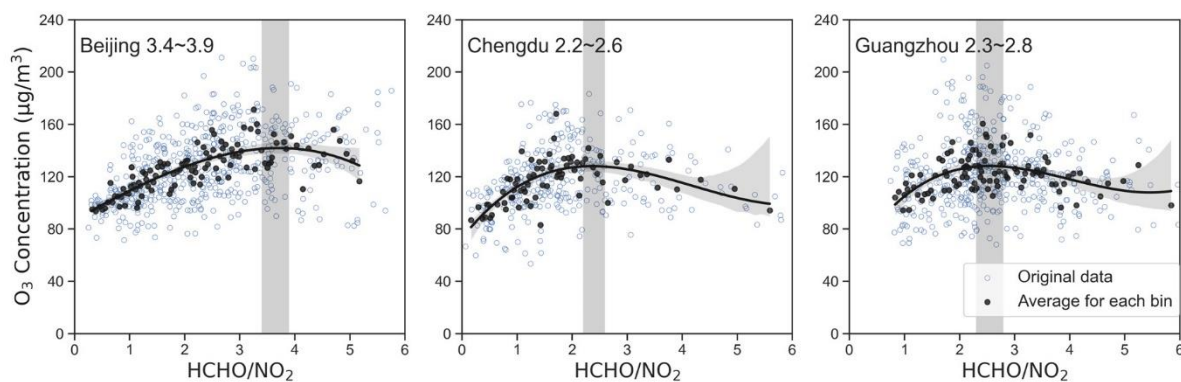
Figure 8: ~~O₃~~ O$_3$ concentration as a function of HCHO/NO$_2$ for all sites in Beijing, Chengdu, and Guangzhou. Black dots and lines are the same as those in Figure 3b but divided into 100 bins, and blue circles are original concentrations.

4 ~~Implication~~ Discussion

Based on the evaluation of the nonlinearity of O$_3$-NO$_x$-VOC chemistry captured by space-based HCHO/NO$_2$, this study derives thresholds marking the transitions between chemical regimes in different regions of China and diagnoses the current spatial distribution of O$_3$ production regimes. The higher resolution TROPOMI satellite data enables a better match between the location of ground-based O$_3$ monitoring stations and the grid of satellite data, thus allowing a more accurate derivation of HCHO/NO$_2$ thresholds and reflection of spatial variations in ozone-NO$_x$-VOC sensitivity.

However, the use of satellite HCHO/NO$_2$ for quantitative diagnosis of ozone-NO$_x$-VOC sensitivity is influenced by the following uncertainties and requires further investigation. First, the thresholds derived from the observation-based approach may be affected by biases in the satellite retrieval algorithm. Satellite instruments measure vertically integrated column densities, and the inhomogeneity of the vertical distribution might impose negative influences (Schroeder et al., 2017). Second, the relationship between satellite-based HCHO and surface VOC reactivity is not fully understood. There are differences in HCHO yields for different classes of VOCs (Shen et al., 2019). Biogenic VOC emissions also have an influence. Since HCHO is a weaker UV-visible absorber than NO$_2$, satellite retrieval of HCHO is more error-prone. These factors may limit their usefulness in detecting HCHO from local sources of anthropogenic VOCs.

Identifying the causes of ozone increases since 2013 is crucial for effectively controlling the ozone pollution in China. The Chinese government has been controlling mainly particulate matter, SO$_2$, and NO$_x$ since 1998 (Zhang et al., 2016). The Air Pollution Prevention and Action Plan, implemented in 2013, aims to reduce the annual average PM$_{2.5}$ concentration by 10% in 2017 compared with 2012 (Chinese State Council, 2013). In 2018, the Chinese government promulgated the Three-Year Action Plan for Winning the Battle of the Blue Sky, which still regards PM$_{2.5}$ control as the primary goal and targets SO$_2$ and NO$_x$ emission reductions (Chinese State Council, 2018). These nationwide emission control measures have decreased PM$_{2.5}$ concentrations rapidly (Xiao et al., 2021) and reduced anthropogenic NO$_x$ emissions. However, the decline in VOC emissions is not yet evident. VOC-limited chemistry exists in most city clusters in China, particularly in built-up areas of cities where air quality monitoring sites are located. Our study highlights that the root cause of ozone increase in major regions is the significant reduction of NO$_x$ alone without effective control of VOC.

and not the concurrent decreases in the PM$_{2.5}$ level as suggested in previous studies (Li et al., 2019), Some studies suggested that the significant decrease in PM$_{2.5}$ is the most crucial factor contributing to the O$_3$ increment in China (Li et al., 2019), but the idea of the impact of HO$_2$ uptake is controversial (Tan et al., 2020). The summertime MDA8 O$_3$ enhancement due to changes in PM$_{2.5}$ levels in NCP during 2013-2017 estimated by Li et al. (1 ppb year^{-1}) is insufficient to explain the observed trend (3.3 ppb year^{-1}) (Lu et al., 2020), which indicates that the effect of PM$_{2.5}$ is not the essential cause of worsening ozone pollution. The simultaneous decline in O$_3$ and PM$_{2.5}$ concentrations in Beijing in recent years (Ren et al., 2021) suggests that appropriate VOC and NO$_x$ emission reductions can control both PM$_{2.5}$ and O$_3$ pollution.

Currently, the VOC-limited regime exists in most major urban clusters in China, which are also areas with high ozone levels. The exploration of the causes of ozone rise in China illustrates the current need for VOC control, which is consistent with the findings of previous studies on major cities and city clusters (Wang et al., 2022; Yang et al., 2019). Deep NO$_x$ reductions will eventually reduce O$_3$ concentrations to lower levels. However, if only NO$_x$ is currently reduced without VOC reductions, O$_3$ concentrations will not be effectively reduced until NO$_x$ is reduced to very low levels, leading to a shift in O$_3$ formation mechanisms toward NO$_x$-limited. This would take a long time and be very costly. In contrast, synergistic control of NO$_x$ and VOC, with a focus on VOC control, is currently a direct and effective approach to alleviate ozone pollution in large cities. and not the concurrent decreases in the PM$_{2.5}$ level as suggested in previous studies (Li et al., 2019).

420 ~~Moreover, the ozone values are high in VOC-limited areas, indicating the necessity of controlling VOC in China. The synergistic control of NOx and VOC, with VOC control as the focus, can help reduce ozone pollution in major cities.~~ ~~The reduction ratio of VOC/NOx can be indicated by the slope of the ridge line of the classic ozone isopleths~~ (Ou et al., 2016; Wang et al., 2019)~~. Based on the method in Fig. 3, O₃ concentrations and the satellite HCHO and NO₂ relationships similar to the O₃ isopleths are obtained. The HCHO/NO₂ value at the peak of the fitted curve is the ratio of HCHO to NO₂ reduction~~

425 ~~for the fastest decrease in O₃ concentration. Three typical developed cities, namely, Beijing in the NCP, Guangzhou in the PRD, and Chengdu in the SCB, are selected to study the reduction pathways, as shown in Fig. 8. The optimal decrease ratio of HCHO to NO₂ is between 2:1 and 4:1, which is 3.4–3.9 for Beijing, 2.2–2.6 for Chengdu, and 2.3–2.8 for Guangzhou. The results obtained by this method roughly reflect the optimal abatement pathways for the two precursors by using the satellite HCHO and NO₂ to represent VOC and NOx. The short-term future O₃ control becomes much more promising in~~

430 ~~terms of enhanced VOC control in urban cities dominated by VOC-limited regimes.~~
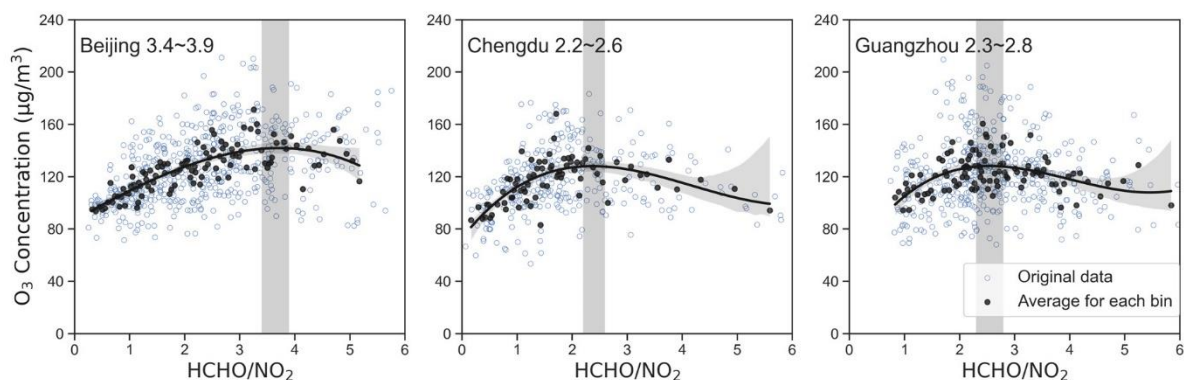
~~Figure 8: O₃ concentration as a function of HCHO/NO₂ for all sites in Beijing, Chengdu, and Guangzhou. Black dots and lines are the same as those in Figure 3b but divided into 100 bins, and blue circles are original concentrations.~~

Data availability

435 The data used in this study can be accessed by contacting the corresponding author, Shaodong Xie (sdxie@pku.edu.cn).

Author contribution

SX and JR initiated the research project. JR performed the data analyses and wrote the manuscript. SX and FG reviewed and revised the paper.

Competing interests

440   The authors declare that they have no conflict of interest.

Acknowledgments

445 **References**

Abbot, D. S., Palmer, P. I., Martin, R. V., Chance, K. V., Jacob, D. J., and Guenther, A.: Seasonal and interannual variability of North American isoprene emissions as determined by formaldehyde column measurements from space, Geophys. Res. Lett., 30, https://doi.org/10.1029/2003GL017336, 2003.

450 Atkinson, R.: Atmospheric chemistry of VOCs and NOx, Atmos. Environ., 34, 2063-2101, https://doi.org/10.1016/S1352-2310(99)00460-4, 2000.

Chang, C., Faust, E., Hou, X., Lee, P., Kim, H. C., Hedquist, B. C., and Liao, K.: Investigating ambient ozone formation regimes in neighboring cities of shale plays in the Northeast United States using photochemical modeling and satellite retrievals, Atmos. Environ., 142, 152-170, https://doi.org/10.1016/j.atmosenv.2016.06.058, 2016.

455 Action plan on air pollution prevention and control (in Chinese): http://www.gov.cn/zwgk/2013-09/12/content_2486773.htm, (last accessed: 7 March 2022), 2013.

Three-year action plan on defending the blue Sky (in Chinese): http://www.gov.cn/zhengce/content/2018-07/03/content_5303158.htm, (last accessed: 7 March 2022), 2018.

Choi, Y., Kim, H., Tong, D., and Lee, P.: Summertime weekly cycles of observed and modeled NOx and O3 concentrations
460 as a function of satellite-derived ozone production sensitivity and land use types over the Continental United States, Atmos. Chem. Phys., 12, 6291-6307, https://doi.org/10.5194/acp-12-6291-2012, 2012.

Duncan, B. N., Yoshida, Y., Damon, M. R., Douglass, A. R., and Witte, J. C.: Temperature dependence of factors controlling isoprene emissions, Geophys. Res. Lett., 36, https://doi.org/10.1029/2008GL037090, 2009.

Duncan, B. N., Yoshida, Y., Olson, J. R., Sillman, S., Martin, R. V., Lamsal, L., Hu, Y., Pickering, K. E., Retscher, C., Allen,
465 D. J., and Crawford, J. H.: Application of OMI observations to a space-based indicator of NOx and VOC controls on surface ozone formation, Atmos. Environ., 44, 2213-2223, https://doi.org/10.1016/j.atmosenv.2010.03.010, 2010.

Jiang, Z., Jolleys, M. D., Fu, T., Palmer, P. I., Ma, Y., Tian, H., Li, J., and Yang, X.: Spatiotemporal and probability variations of surface PM2.5 over China between 2013 and 2019 and the associated changes in health risks: An integrative observation and model analysis, Sci. Total Environ., 723, 137896, https://doi.org/10.1016/j.scitotenv.2020.137896, 2020.

470 Jin, X., Fiore, A. M., Murray, L. T., Valin, L. C., Lamsal, L. N., Duncan, B., Folkert Boersma, K., De Smedt, I., Abad, G. G., Chance, K., and Tonnesen, G. S.: Evaluating a Space-Based Indicator of Surface Ozone-NOx-VOC Sensitivity Over Midlatitude Source Regions and Application to Decadal Trends, Journal of Geophysical Research: Atmospheres, 122, 10, 410-439, 461, https://doi.org/10.1002/2017JD026720, 2017.

Jin, X., Fiore, A., Boersma, K. F., De Smedt, I., and Valin, L.: Inferring Changes in Summertime Surface Ozone-NOx-VOC
475 Chemistry over US Urban Areas from Two Decades of Satellite and Ground-Based Observations, Environ. Sci. Technol., 54, 6518-6529, https://doi.org/10.1021/acs.est.9b07785, 2020.

Jin, X., and Holloway, T.: Spatial and temporal variability of ozone sensitivity over China observed from the Ozone

Monitoring Instrument, Journal of Geophysical Research: Atmospheres, 120, 7229-7246, https://doi.org/10.1002/2015JD023250, 2015.

480   KLEINMAN, L. I.: Low and high NOx tropospheric photochemistry, JOURNAL OF GEOPHYSICAL RESEARCH-ATMOSPHERES, 99, 16831-16838, https://doi.org/10.1029/94JD01028, 1994.

Lamsal, L. N., Krotkov, N. A., Celarier, E. A., Swartz, W. H., Pickering, K. E., Bucsela, E. J., Gleason, J. F., Martin, R. V., Philip, S., Irie, H., Cede, A., Herman, J., Weinheimer, A., Szykman, J. J., and Knepp, T. N.: Evaluation of OMI operational standard NO2 column retrievals using in situ and surface-based NO2 observations, Atmos. Chem. Phys., 14,

485   11587-11609, https://doi.org/10.5194/acp-14-11587-2014, 2014.

Le, T., Wang, Y., Liu, L., Yang, J., Yung, Y. L., Li, G., and Seinfeld, J. H.: Unexpected air pollution with marked emission reductions during the COVID-19 outbreak in China, Science, 369, 702, https://doi.org/10.1126/science.abb7431, 2020.

Li, D. R., Wang, S. S., Xue, R. B., Zhu, J., Zhang, S. B., Sun, Z. B., and Zhou, B.: OMI-observed HCHO in Shanghai, China, during 2010-2019 and ozone sensitivity inferred by an improved HCHO/NO2 ratio, Atmos. Chem. Phys., 21, 15447-

490   15460, https://doi.org/10.5194/acp-21-15447-2021, 2021.

Li, K., Jacob, D. J., Liao, H., Shen, L., Zhang, Q., and Bates, K. H.: Anthropogenic drivers of 2013-2017 trends in summer surface ozone in China, P. Natl. Acad. Sci. Usa., 116, 422-427, https://doi.org/10.1073/pnas.1812168116, 2019.

Li, K., Jacob, D. J., Shen, L., Lu, X., De Smedt, I., and Liao, H.: Increases in surface ozone pollution in China from 2013 to 2019: anthropogenic and meteorological influences, Atmos. Chem. Phys., 20, 11423-11433, https://doi.org/10.5194/acp-

495   20-11423-2020, 2020.

Li, L. Y., Yang, W. Z., Xie, S. D., and Wu, Y.: Estimations and uncertainty of biogenic volatile organic compound emission inventory in China for 2008?2018, Sci. Total Environ., 733, https://doi.org/10.1016/j.scitotenv.2020.139301, 2020.

Li, R. Y., Xu, M. Q., Li, M. C., Chen, Z. Y., Zhao, N., Gao, B. B., and Yao, Q.: Identifying the spatiotemporal variations in ozone formation regimes across China from 2005 to 2019 based on polynomial simulation and causality analysis, Atmos.

500   Chem. Phys., 21, 15631-15646, https://doi.org/10.5194/acp-21-15631-2021, 2021.

Liang, X. M., Chen, L. G., Liu, M., Lu, Q., Lu, H. T., Gao, B., Zhao, W., Sun, X. B., Xu, J. T., and Ye, D. Q.: Carbonyls from commercial, canteen and residential cooking activities as crucial components of VOC emissions in China, Sci. Total Environ., 846, https://doi.org/10.1016/j.scitotenv.2022.157317, 2022.

Lin, N., Wang, Y., Zhang, Y., and Yang, K.: A large decline of tropospheric NO2 in China observed from space by SNPP

505   OMPS, Sci. Total Environ., 675, 337-342, https://doi.org/10.1016/j.scitotenv.2019.04.090, 2019.

Liu, C., and Shi, K.: A review on methodology in O3-NOx-VOC sensitivity study, Environ. Pollut., 291, https://doi.org/10.1016/j.envpol.2021.118249, 2021.

Lu, X., Hong, J., Zhang, L., Cooper, O. R., Schultz, M. G., Xu, X., Wang, T., Gao, M., Zhao, Y., and Zhang, Y.: Severe Surface Ozone Pollution in China: A Global Perspective, Environmental Science & Technology Letters, 5, 487-494,

510   https://doi.org/10.1021/acs.estlett.8b00366, 2018.

Lu, X., Zhang, L., Wang, X., Gao, M., Li, K., Zhang, Y., Yue, X., and Zhang, Y.: Rapid Increases in Warm-Season Surface

Ozone and Resulting Health Impact in China Since 2013, Environmental Science & Technology Letters, 7, 240-247, https://doi.org/10.1021/acs.estlett.0c00171, 2020.

Martin, R. V.: Global inventory of nitrogen oxide emissions constrained by space-based observations of NO2 columns, Journal of Geophysical Research, 108, https://doi.org/10.1029/2003JD003453, 2003.

Martin, R. V., Fiore, A. M., and Van Donkelaar, A.: Space-based diagnosis of surface ozone sensitivity to anthropogenic emissions, Geophys. Res. Lett., 31, https://doi.org/10.1029/2004GL019416, 2004.

Nelson, B. S., Stewart, G. J., Drysdale, W. S., Newland, M. J., Vaughan, A. R., Dunmore, R. E., Edwards, P. M., Lewis, A. C., Hamilton, J. F., Acton, W. J., Hewitt, C. N., Crilley, L. R., Alam, M. S., Sahin, U. A., Beddows, D. C. S., Bloss, W. J., Slater, E., Whalley, L. K., Heard, D. E., Cash, J. M., Langford, B., Nemitz, E., Sommariva, R., Cox, S., Shivani, Gadi, R., Gurjar, B. R., Hopkins, J. R., Rickard, A. R., and Lee, J. D.: In situ ozone production is highly sensitive to volatile organic compounds in Delhi, India, Atmos. Chem. Phys., 21, 13609-13630, https://doi.org/10.5194/acp-21-13609-2021, 2021.

Ou, J., Yuan, Z., Zheng, J., Huang, Z., Shao, M., Li, Z., Huang, X., Guo, H., and Louie, P. K. K.: Ambient Ozone Control in a Photochemically Active Region: Short-Term Despiking or Long-Term Attainment? Environ. Sci. Technol., 50, 5720-5728, https://doi.org/10.1021/acs.est.6b00345, 2016.

Pei, C., Yang, W., Zhang, Y., Song, W., Xiao, S., Wang, J., Zhang, J., Zhang, T., Chen, D., Wang, Y., Chen, Y., and Wang, X.: Decrease in ambient volatile organic compounds during the COVID-19 lockdown period in the Pearl River Delta region, south China., The Science of the total environment, 153720, https://doi.org/10.1016/j.scitotenv.2022.153720, 2022.

Pusede, S. E., Steiner, A. L., and Cohen, R. C.: Temperature and Recent Trends in the Chemistry of Continental Surface Ozone, Chem. Rev., 115, 3898-3918, https://doi.org/10.1021/cr5006815, 2015.

Ren, J., Hao, Y., Simayi, M., Shi, Y., and Xie, S.: Spatiotemporal variation of surface ozone and its causes in Beijing, China since 2014, Atmos. Environ., 260, https://doi.org/10.1016/j.atmosenv.2021.118556, 2021.

Schroeder, J. R., Crawford, J. H., Fried, A., Walega, J., Weinheimer, A., Wisthaler, A., Muller, M., Mikoviny, T., Chen, G., Shook, M., Blake, D. R., and Tonnesen, G. S.: New insights into the column CH2O/NO2 ratio as an indicator of near-surface ozone sensitivity, JOURNAL OF GEOPHYSICAL RESEARCH-ATMOSPHERES, 122, 8885-8907, https://doi.org/10.1002/2017JD026781, 2017.

Shen, H., Sun, Z., Chen, Y., Russell, A. G., Hu, Y., Odman, M. T., Qian, Y., Archibald, A. T., and Tao, S.: Novel Method for Ozone Isopleth Construction and Diagnosis for the Ozone Control Strategy of Chinese Cities, Environ. Sci. Technol., 55, 15625-15636, https://doi.org/10.1021/acs.est.1c01567, 2021.

Shen, L., Jacob, D. J., Zhu, L., Zhang, Q., Zheng, B., Sulprizio, M. P., Li, K., De Smedt, I., Abad, G. G., Cao, H., Fu, T., and Liao, H.: The 2005-2016 Trends of Formaldehyde Columns Over China Observed by Satellites: Increasing Anthropogenic Emissions of Volatile Organic Compounds and Decreasing Agricultural Fire Emissions, Geophys. Res. Lett., 46, 4468-4475, https://doi.org/10.1029/2019GL082172, 2019.

SILLMAN, S.: THE USE OF NOY, H2O2, AND HNO3 AS INDICATORS FOR OZONE-NOX-HYDROCARBON SENSITIVITY IN URBAN LOCATIONS, JOURNAL OF GEOPHYSICAL RESEARCH-ATMOSPHERES, 100, 14175-14188, https://doi.org/10.1029/94JD02953, 1995.

Sillman, S.: The relation between ozone, NOx and hydrocarbons in urban and polluted rural environments, Atmos. Environ., 33, 1821-1845, https://doi.org/10.1016/S1352-2310(98)00345-8, 1999.

Sillman, S., Logan, J. A., and Wofsy, S. C.: The sensitivity of ozone to nitrogen oxides and hydrocarbons in regional ozone episodes, Journal of Geophysical Research: Atmospheres, 95, 1837-1851, https://doi.org/10.1029/JD095iD02p01837, 1990.

Sillman, S., and He, D. Y.: Some theoretical results concerning O-3-NOx-VOC chemistry and NOx-VOC indicators, JOURNAL OF GEOPHYSICAL RESEARCH-ATMOSPHERES, 107, https://doi.org/10.1029/2001JD001123, 2002.

Simayi, M., Shi, Y., Xi, Z., Ren, J., Hini, G., and Xie, S.: Emission trends of industrial VOCs in China since the clean air action and future reduction perspectives, Sci. Total Environ., 826, 153994, https://doi.org/10.1016/j.scitotenv.2022.153994, 2022.

Song, M., Feng, M., Li, X., Tan, Q., Song, D., Liu, H., Dong, H., Zeng, L., Lu, K., and Zhang, Y.: Causes and sources of heavy ozone pollution in Chengdu (in Chinese), China Environmental Science, 42, 1057-1065, 2022.

Souri, A. H., Nowlan, C. R., Wolfe, G. M., Lamsal, L. N., Chan Miller, C. E., Abad, G. G., Janz, S. J., Fried, A., Blake, D. R., Weinheimer, A. J., Diskin, G. S., Liu, X., and Chance, K.: Revisiting the effectiveness of HCHO/NO2 ratios for inferring ozone sensitivity to its precursors using high resolution airborne remote sensing observations in a high ozone episode during the KORUS-AQ campaign, Atmos. Environ., 224, 117341, https://doi.org/10.1016/j.atmosenv.2020.117341, 2020.

Tan, Z., Hofzumahaus, A., Lu, K., Brown, S. S., Holland, F., Huey, L. G., Kiendler-Scharr, A., Li, X., Liu, X., Ma, N., Min, K., Rohrer, F., Shao, M., Wahner, A., Wang, Y., Wiedensohler, A., Wu, Y., Wu, Z., Zeng, L., Zhang, Y., and Fuchs, H.: No Evidence for a Significant Impact of Heterogeneous Chemistry on Radical Concentrations in the North China Plain in Summer 2014, Environ. Sci. Technol., 54, 5973-5979, https://doi.org/10.1021/acs.est.0c00525, 2020.

Tan, Z., Lu, K., Jiang, M., Su, R., Dong, H., Zeng, L., Xie, S., Tan, Q., and Zhang, Y.: Exploring ozone pollution in Chengdu, southwestern China: A case study from radical chemistry to O3-VOC-NOx sensitivity, Sci. Total Environ., 636, 775-786, https://doi.org/10.1016/j.scitotenv.2018.04.286, 2018.

Veefkind, J. P., Aben, I., McMullan, K., Forster, H., de Vries, J., Otter, G., Claas, J., Eskes, H. J., de Haan, J. F., Kleipool, Q., van Weele, M., Hasekamp, O., Hoogeveen, R., Landgraf, J., Snel, R., Tol, P., Ingmann, P., Voors, R., Kruizinga, B., Vink, R., Visser, H., and Levelt, P. F.: TROPOMI on the ESA Sentinel-5 Precursor: A GMES mission for global observations of the atmospheric composition for climate, air quality and ozone layer applications, Remote Sens. Environ., 120, 70-83, https://doi.org/10.1016/j.rse.2011.09.027, 2012.

Wang, N., Lyu, X., Deng, X., Huang, X., Jiang, F., and Ding, A.: Aggravating O3 pollution due to NOx emission control in eastern China, Sci. Total Environ., 677, 732-744, https://doi.org/10.1016/j.scitotenv.2019.04.388, 2019.

580   Wang, T., Xue, L., Brimblecombe, P., Lam, Y. F., Li, L., and Zhang, L.: Ozone pollution in China: A review of concentrations, meteorological influences, chemical precursors, and effects, Sci. Total Environ., 575, 1582-1596, https://doi.org/10.1016/j.scitotenv.2016.10.081, 2017.

Wang, W. J., Parrish, D. D., Wang, S. W., Bao, F. X., Ni, R. J., Li, X., Yang, S. D., Wang, H. L., Cheng, Y. F., and Su, H.: Long-term trend of ozone pollution in China during 2014-2020: distinct seasonal and spatial characteristics and ozone

585   sensitivity, Atmos. Chem. Phys., 22, 8935-8949, https://doi.org/10.5194/acp-22-8935-2022, 2022.

Wang, W. N., Ronald, V., Ding, J. Y., van Weele, M., and Cheng, T. H.: Spatial and temporal changes of the ozone sensitivity in China based on satellite and ground-based observations, Atmos. Chem. Phys., 21, 7253-7269, https://doi.org/10.5194/acp-21-7253-2021, 2021.

Wang, X., Fu, T., Zhang, L., Cao, H., Zhang, Q., Ma, H., Shen, L., Evans, M. J., Ivatt, P. D., Lu, X., Chen, Y., Zhang, L.,

590   Feng, X., Yang, X., Zhu, L., and Henze, D. K.: Sensitivities of Ozone Air Pollution in the Beijing–Tianjin–Hebei Area to Local and Upwind Precursor Emissions Using Adjoint Modeling, Environ. Sci. Technol., 55, 5752-5762, https://doi.org/10.1021/acs.est.1c00131, 2021.

Williams, J. E., Boersma, K. F., Le Sager, P., and Verstraeten, W. W.: The high-resolution version of TM5-MP for optimized satellite retrievals: description and validation, Geosci. Model Dev., 10, 721-750, https://doi.org/10.5194/gmd-

595   10-721-2017, 2017.

Wolfe, G. M., Kaiser, J., Hanisco, T. F., Keutsch, F. N., de Gouw, J. A., Gilman, J. B., Graus, M., Hatch, C. D., Holloway, J., Horowitz, L. W., Lee, B. H., Lerner, B. M., Lopez-Hilifiker, F., Mao, J., Marvin, M. R., Peischl, J., Pollack, I. B., Roberts, J. M., Ryerson, T. B., Thornton, J. A., Veres, P. R., and Warneke, C.: Formaldehyde production from isoprene oxidation across NOx regimes, Atmos. Chem. Phys., 16, 2597-2610, https://doi.org/10.5194/acp-16-2597-2016, 2016.

600   World Health Organization: WHO's global air-quality guidelines0140-6736, 2021.

Xiao, Q., Geng, G., Xue, T., Liu, S., Cai, C., He, K., and Zhang, Q.: Tracking PM2.5 and O-3 Pollution and the Related Health Burden in China 2013-2020, Environ. Sci. Technol., https://doi.org/10.1021/acs.est.1c04548, 2021.

Yang, L., Luo, H., Yuan, Z., Zheng, J., Huang, Z., Li, C., Lin, X., Louie, P. K. K., Chen, D., and Bian, Y.: Quantitative impacts of meteorology and precursor emission changes on the long-term trend of ambient ozone over the Pearl River

605   Delta, China, and implications for ozone control strategy, Atmos. Chem. Phys., 19, 12901-12916, https://doi.org/10.5194/acp-19-12901-2019, 2019.

Zhang, H., Wang, S., Hao, J., Wang, X., Wang, S., Chai, F., and Li, M.: Air pollution and control action in Beijing, J. Clean. Prod., 112, 1519-1527, https://doi.org/10.1016/j.jclepro.2015.04.092, 2016.

Zhang, Q., Zheng, Y., Tong, D., Shao, M., Wang, S., Zhang, Y., Xu, X., Wang, J., He, H., Liu, W., Ding, Y., Lei, Y., Li, J.,

610   Wang, Z., Zhang, X., Wang, Y., Cheng, J., Liu, Y., Shi, Q., Yan, L., Geng, G., Hong, C., Li, M., Liu, F., Zheng, B., Cao, J., Ding, A., Gao, J., Fu, Q., Huo, J., Liu, B., Liu, Z., Yang, F., He, K., and Hao, J.: Drivers of improved PM2.5 air quality in China from 2013 to 2017, P. Natl. Acad. Sci. Usa., 116, 24463-24469, https://doi.org/10.1073/pnas.1907956116, 2019.

Zhao, S., Yin, D., Yu, Y., Kang, S., Qin, D., and Dong, L.: PM2.5 and O3 pollution during 2015–2019 over 367 Chinese

cities: Spatiotemporal variations, meteorological and topographical impacts, Environ. Pollut., 264, 114694, https://doi.org/10.1016/j.envpol.2020.114694, 2020.

Zheng, B., Tong, D., Li, M., Liu, F., Hong, C., Geng, G., Li, H., Li, X., Peng, L., Qi, J., Yan, L., Zhang, Y., Zhao, H., Zheng, Y., He, K., and Zhang, Q.: Trends in China's anthropogenic emissions since 2010 as the consequence of clean air actions, Atmos. Chem. Phys., 18, 14095-14111, https://doi.org/10.5194/acp-18-14095-2018, 2018a.

Zheng, B., Tong, D., Li, M., Liu, F., Hong, C., Geng, G., Li, H., Li, X., Peng, L., Qi, J., Yan, L., Zhang, Y., Zhao, H., Zheng, Y., He, K., and Zhang, Q.: Trends in China's anthropogenic emissions since 2010 as the consequence of clean air actions, Atmos. Chem. Phys., 18, 14095-14111, https://doi.org/10.5194/acp-18-14095-2018, 2018b.

Zhu, L., Jacob, D. J., Mickley, L. J., Marais, E. A., Cohan, D. S., Yoshida, Y., Duncan, B. N., Abad, G. G., and Chance, K. V.: Anthropogenic emissions of highly reactive volatile organic compounds in eastern Texas inferred from oversampling of satellite (OMI) measurements of HCHO columns, Environ. Res. Lett., 9, https://doi.org/10.1088/1748-9326/9/11/114004, 2014.

Zhu, L., Mickley, L. J., Jacob, D. J., Marais, E. A., Sheng, J., Hu, L., Abad, G. G., and Chance, K.: Long-term (2005-2014) trends in formaldehyde (HCHO) columns across North America as seen by the OMI satellite instrument: Evidence of changing emissions of volatile organic compounds, Geophys. Res. Lett., 44, 7079-7086, https://doi.org/10.1002/2017GL073859, 2017.